

Resonances and Multistability in Josephson Junction Connected to a Resonator

Denis S. Goldobin^{1,2,*} and Lyudmila S. Klimenko^{1,2}

¹Institute of Continuous Media Mechanics, Ural Branch of RAS, Perm, 614013, Russia

²Department of Theoretical Physics, Perm State University, Perm, 614990, Russia

*Denis.Goldobin@gmail.com

ABSTRACT

We study the dynamics of a Josephson junction connected to a dc current supply via distributed parameter capacitor, which serves as a resonator. We reveal multistability in the current–voltage characteristic of the system; this multistability is related to resonances between the generated frequency and the resonator. The resonant pattern requires detailed consideration, in particular, because its basic features may be similar to those of patterns reported for arrays of Josephson junctions demonstrating coherent stimulated emission in the experimental work [P. Barbara, *et al.*, Phys. Rev. Lett. **82**, 1963 (1999)]. From the viewpoint of nonlinear dynamics, the resonances between a Josephson junction and a resonator are of interest because of specificity of the former; its oscillation frequency is directly governed by control parameters of the system and can vary in a wide range. Our analytical results are in a good agreement with the results of numerical simulations.

Introduction

Josephson junction—a contact between two superconductors optionally separated by a thin insulator layer—is a macroscopic element the dynamics of which is essentially quantum one^{1,2}. These elements are natural voltage-to-frequency transducers. One can distinguish two regimes of operation of a Josephson junction: direct supercurrent with zero voltage applied across a junction and oscillations of supercurrent when the voltage is non-zero. The oscillation cyclic frequency for a dc voltage V_{dc} is $\omega = 2eV_{dc}/\hbar$, where e is the electron charge and \hbar is the Planck constant, and noteworthy indicates that charge carriers in superconductors are Cooper pairs.

Interconnected Josephson junctions were predicted to be able to self-synchronize with a common radiation field and emit coherently³. The suggested synchronization mechanism was a quantum one and analogous to the one in the case of superradiant atoms in resonant cavity. Even more similarity between these two quantum systems was revealed with farther studies^{4,5}.

Later on, observations of coherent emission for one- and two-dimensional arrays of junctions were reported^{6,7}, although the underlying synchronization mechanism was shown to be a classical one^{6,8}. Barbara *et al.*⁹ presented observations for two-dimensional arrays of Josephson junctions (see Figure 1), where stimulated emission was causing coherence. These observations could not be explained by classical coupling mechanisms and experimentally confirmed the predictions from Tilley³ and Rogovin and Scully⁴.

It is interesting, that the electric circuit used in experiments by Barbara *et al.*⁹ contained a capacitor which could serve as a resonator with distributed parameters under certain conditions. All the components of the circuit were high- Q elements. Although their conclusions of the paper⁹ are solid, the question of interaction of a single Josephson junction with a resonator requires subtle treatment. As we will show below, the current–voltage characteristic of the latter system exhibits patterns with

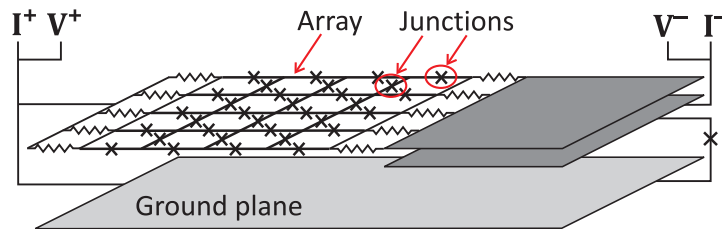


Figure 1. Circuit of the array of Josephson junctions connected to an extensive capacitor used by Barbara *et al.*⁹

multiple resonances which are different from the patterns reported for coherent states of junction array only in details; if one infers the expected qualitative properties of these characteristics, they will be similar. To distinguish these patterns from one another surely one needs a good understanding of both patterns. In this paper, we provide the study of the current–voltage characteristics of a single high- Q Josephson junction connected with a high- Q resonator.

In a high- Q distributed parameter capacitor, the signals propagate with nearly no dispersion and decay. The interaction of self-sustained nonlinear oscillators with a neutrally stable dispersion-free waveguide is known to be able to lead to a rich and complex resonant dynamics¹⁰. From the viewpoint of nonlinear dynamics, Josephson junction is a nonlinear oscillator with a very special property: its oscillation frequency in the ac mode is directly governed by a control parameter, the input current². Though for the majority of nonlinear oscillators the frequency depends on the oscillation amplitude and control parameters, its variation is restricted to a certain range which rarely exceeds a few octaves. Hence, for the dynamics of a given nonlinear oscillator connected to a resonator, only a few or even none of resonant frequencies can be relevant. In contrast, the oscillation frequency of a Josephson junction oscillator varies nearly linearly with the input current, and any resonant frequencies are accessible and relevant as operation modes. Thus, additionally to the necessity to distinguish resonant patterns of different nature, the dynamics of a single Josephson junction connected to a resonator is of interest and deserves attention itself.

From the engineering point of view, the resonances in the system under our consideration are important for operation of Josephson junction as a voltage-to-frequency or current-to-frequency transducer¹¹; they can either affect susceptibility of the system to control or enhance the stability of generated frequencies.

Pairs of Josephson junctions with capacitive coupling were also suggested for design of superconducting qubits^{12–14}. In this relation, any information on possible effects emerging due to nonlocality of the capacitor connected to a Josephson junction will be beneficial.

In this paper we derive the governing equations for the Josephson junction connected to a resonator (distributed parameter capacitor). Then the analytical solutions are obtained for the case of high generation frequency (*or* high input current) and low energy dissipation and confirmed with the results of numerical simulations. Further, we develop the weakly nonlinear analysis, which explains non-linear resonances observed with numerical simulation at low frequencies. Finally, we discuss the results and derive conclusions.

Josephson junction with resonator

Basic physical and mathematical model

Let us consider an elongate resonator (distributed parameter capacitor) of length l along the x -axis, connected to the Josephson junction at $x = 0$ and an external current supply at $x = l$. The inductance L , the capacity c , the resistance r for the current along the resonator, and the conductance σ for the leakage current between its plates are distributed as shown in Figure 2. For the infinitesimal interval dx the voltage increment du and the current increment di are

$$du = dLi_t + dri, \quad di = dcu_t + d\sigma u, \quad (1)$$

where subscript t indicates the partial time derivative. Hence,

$$i_t + r_x L_x^{-1} i = L_x^{-1} u_x, \quad u_t + \sigma_x c_x^{-1} u = c_x^{-1} i_x, \quad (2)$$

where subscript x indicates the partial x -derivative; L_x , c_x , r_x and σ_x are the inductance, capacity, resistance and leakage conductance per the unit length of the capacitor, respectively.

The net current I through the Josephson junction is contributed by the tunnelling current $I_0 \sin \phi$, the leakage current U/R , and the bias current $C(dU/dt)$ due to the junction electrical capacity²;

$$I = I_0 \sin \phi + \frac{U}{R} + CU_t, \quad \phi_t = \frac{2e}{\hbar} U, \quad (3)$$

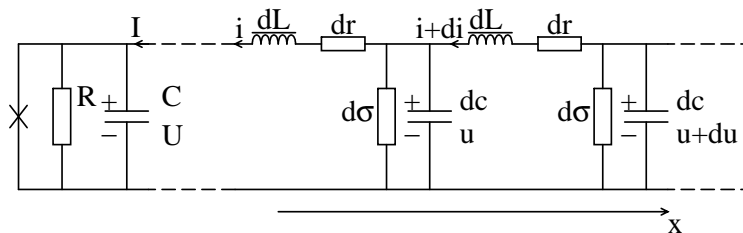


Figure 2. Josephson junction connected to a resonator with distributed capacity, induction, and ohmic resistance

where U is the potential drop on the junction, ϕ is the phase difference across the junction of the Ginzburg–Landau complex order parameter associated to the macroscopic current in a superconductor, I_0 is determined by physical properties of the junction, R is the ohmic resistance of the junction, C is the junction capacity, e is the elementary charge, \hbar is the Planck constant.

It is convenient to make the following rescaling of coordinates and variables and introduce dimensionless parameters:

$$\begin{aligned} x &= l\tilde{x}, & t &= t_*\tilde{t}, & I &= I_0\tilde{I}, & U &= U_*\tilde{U}, & t_* &= \sqrt{\frac{\hbar C}{2eI_0}}, & U_* &= I_0\sqrt{\frac{L_x}{c_x}}, \\ v &= \frac{t_*}{l\sqrt{c_x L_x}}, & \gamma_i &= \frac{r_x}{L_x}t_*, & \gamma_u &= \frac{\sigma_x}{c_x}t_*, & 2\beta &= \frac{t_*}{RC}, & F &= \frac{\hbar}{2et_*U_*} = \left[\frac{2e}{\hbar} \frac{C}{c_x} L_x I_0 \right]^{-\frac{1}{2}}. \end{aligned} \quad (4)$$

Henceforth, the sign tilde is omitted.

In dimensionless form, Eqs. (2) and (3) constitute the governing equation system with distributed parameters (one-dimensional) and boundary conditions:

$$u_t + \gamma_u u = v i_x, \quad (5)$$

$$i_t + \gamma_i i = v u_x, \quad (6)$$

$$x = 0: \quad i(0, t) = \sin \phi + 2\beta \phi_t + \phi_{tt}, \quad (7)$$

$$\phi_t = F^{-1} u(0, t), \quad (8)$$

$$x = 1: \quad i(1, t) = I_1(t), \quad (9)$$

where $I_1(t)$ is the external input current.

Waves in resonator

We first focus on the case of $\gamma_i = \gamma_u = \gamma$. In this case we can seek for an analytical solution in form of a pair of counterpropagating decaying waves;

$$i(x, t) = e^{-\gamma t} (g(t - x/v) + h(t + x/v)). \quad (10)$$

Eq. (9) yields

$$h(t) = I_1(t - T) e^{\gamma(t-T)} - g(t - 2T), \quad (11)$$

where $T = v^{-1}$. Substituting the latter equation into Eq. (10), one can find

$$i(x, t) = I_1(t - T + x/v) e^{-\gamma(T-x/v)} + e^{-\gamma t} (g(t - x/v) - g(t - 2T + x/v)). \quad (12)$$

One can seek for $u(x, t)$ in the same form as $i(x, t)$; specifically, $u(x, t) = e^{-\gamma t} (g_1(t - x/v) + h_1(t + x/v))$. From Eq. (5) or Eq. (6), $g'_1(\xi) = -g'(\xi)$ and $h'_1(\xi) = h'(\xi)$ (here the prime denotes derivative); therefore,

$$u(x, t) = e^{-\gamma t} (-g(t - x/v) + h(t + x/v) + \text{const}), \quad (13)$$

where const can be set to zero by renormalization of g and h . Substituting h , one obtains

$$u(x, t) = I_1(t - T + x/v) e^{-\gamma(T-x/v)} + e^{-\gamma t} (-g(t - x/v) - g(t - 2T + x/v)). \quad (14)$$

For the general case of $\gamma_i \neq \gamma_u$ and a weakly dissipative resonator (which is of practical interest), i.e., $\gamma_i \ll v$ and $\gamma_u \ll v$, Eqs. (12) and (14) are still valid with

$$\gamma = \frac{\gamma_i + \gamma_u}{2}$$

up to corrections $\mathcal{O}((\gamma_i - \gamma_u)^2/v^2)$.

Dynamics of Josephson junction

Now we can rewrite the governing equations of our dynamic system in a null-dimensional form with recursive delay feedback. Using Eq. (14) one can rewrite Eqs. (7) and (8) as

$$\phi_{tt}(t) + 2\beta\phi_t(t) + \sin\phi(t) = I_1(t-T)e^{-\gamma T} + f(t) - e^{-2\gamma T}f(t-2T), \quad (15)$$

$$F\phi_t(t) = I_1(t-T)e^{-\gamma T} - f(t) - e^{-2\gamma T}f(t-2T), \quad (16)$$

where $f(t) = e^{-\gamma t}g(t)$. In an alternative form,

$$\phi_{tt}(t) + (2\beta + F)\phi_t(t) + \sin\phi(t) = 2 \sum_{n=0}^{\infty} (-1)^n e^{-(2n+1)\gamma T} I_1(t - (2n+1)T) - 2F \sum_{n=1}^{\infty} (-1)^n e^{-2n\gamma T} \phi_t(t - 2nT). \quad (17)$$

For a constant in time input current $I_1(t) = I_1$ the first sum in Eq. (17) $\sum_{n=0}^{\infty} (-1)^n e^{-(2n+1)\gamma T} = (2 \cosh \gamma T)^{-1}$; thus one obtains

$$\phi_{tt}(t) + (2\beta + F)\phi_t(t) + \sin\phi(t) = \frac{I_1}{\cosh \gamma T} - 2F \sum_{n=1}^{\infty} (-1)^n e^{-2n\gamma T} \phi_t(t - 2nT). \quad (18)$$

The nonlinear differential equation (18) with a linear recursive delay feedback governs the dynamics of the system we consider. Our further study is focused on solving this equation, examining properties of its solution, and their interpretation.

Average (measured) input voltage. Let us consider the average value of the input voltage, which can be treated as a measured input voltage as oscillations about this value are high-frequency ones,

$$V_1 = \langle u(1) \rangle = \langle I_1(t) - 2e^{-\gamma t}f(t-T) \rangle, \quad (19)$$

where $\langle \dots \rangle$ denotes averaging over time. From Eq. (16), one can find

$$-e^{-\gamma T}f(t-T) = \sum_{n=1}^{\infty} [I_1(t-2nT)e^{-2n\gamma T}(-1)^n - F\phi_t(t-(2n-1)T)e^{-(2n-1)\gamma T}(-1)^n]. \quad (20)$$

Since $\langle \phi_t \rangle$ is constant in time by definition, Eqs. (19) and (20) yield

$$V_1 = I_1 \tanh 2\gamma T + \frac{F\langle \phi_t \rangle}{\cosh \gamma T}. \quad (21)$$

The case of high input current

When the net current I through the junction is large compared to the maximal tunnelling current I_0 [see Eq. (3)], the ohmic contribution in the current is dominating. The nearly constant ohmic current yields a nearly constant voltage U across the junction and, according to Eq. (3), phase $\phi(t)$ rotates quickly with some oscillations about the linear growth trend; one can seek for the solution in form

$$\phi(t) = \phi_0 + \omega t + a \cos \omega t + \dots, \quad (22)$$

assuming $I_1 \gg 1$, $\omega \gg 1$ and $a \ll 1$, where the dots stand for higher-order harmonics, which are to be neglected. The term $\sin \omega t$ is removed by means of shifting the time offset; this shift is represented by constant ϕ_0 , which is yet to be found.

For calculation of $\sin \phi$ in Eq. (18), we employ the Jacobi–Anger expansion;

$$\cos(a \cos \omega t) = J_0(a) + 2 \sum_{n=1}^{\infty} (-1)^n J_{2n}(a) \cos 2n\omega t, \quad \sin(a \cos \omega t) = 2 \sum_{n=0}^{\infty} (-1)^n J_{2n+1}(a) \cos (2n+1)\omega t,$$

where $J_n(a)$ is the n -th order Bessel function of the first kind. Keeping only the constant-in-time term and the first harmonics in the Jacobi–Anger expansion, one finds

$$\begin{aligned} \sin \phi &= \sin(\phi_0 + \omega t) \cos(a \cos \omega t) + \cos(\phi_0 + \omega t) \sin(a \cos \omega t) \\ &= J_1(a) \cos \phi_0 + J_0(a) \cos \phi_0 \sin \omega t + J_0(a) \sin \phi_0 \cos \omega t + \dots \end{aligned} \quad (23)$$

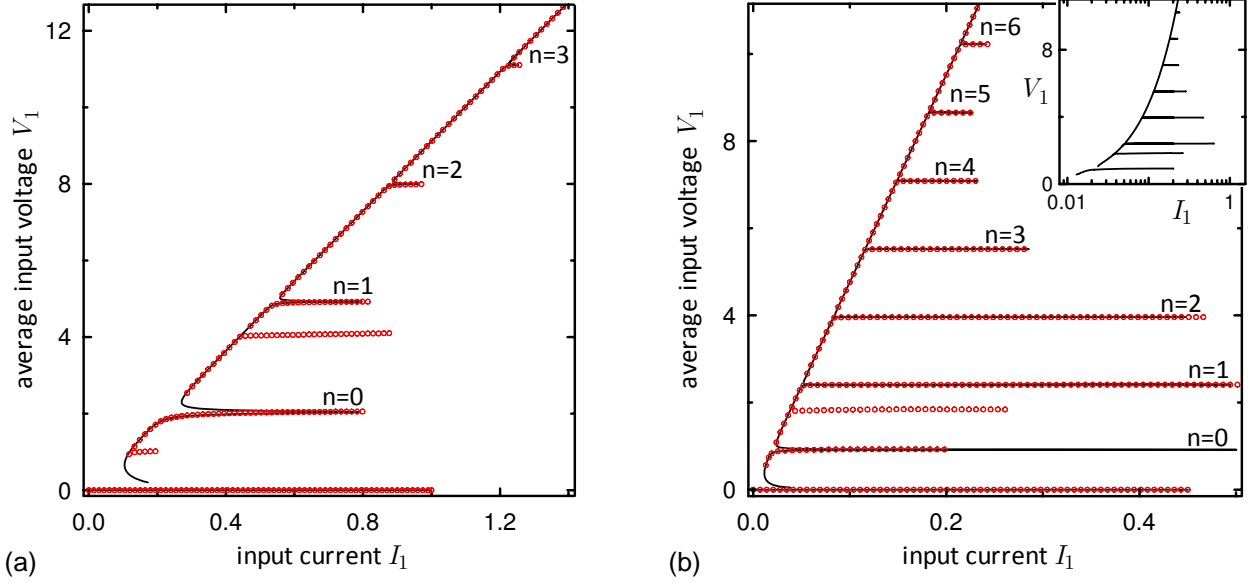


Figure 3. The current–voltage characteristic is plotted for (a) $\beta = 0.05$, $\gamma = 0.01$, $F = 1$; (b) $\beta = 0.005$, $\gamma = 0.001$, $F = 0.5$. The average input voltage V_1 is determined by Eq. (21). Red circles: the results of numerical simulation of Eq. (18), black solid line: the analytical solution (28)–(29). In the insert graph the same current–voltage characteristic from numerical simulations is plotted with the log–linear scale to show the properties of peaks at nonlarge values of V_1 . For non-large values of V , one can notice two small sharp stripes in numerical results deviating from the analytical solution; analytical description of these stripes requires the higher order corrections to be accounted for. With a recursive delay feedback, even weak anharmonicity is known to be able to lead to strong resonant effects¹⁵. However, for moderate and large values of V_1 these high-order resonances are not detectable and the analytical theory describes the system dynamics well.

Then Eq. (18) reads

$$\begin{aligned}
 & -\omega^2 a \cos \omega t + (2\beta + F)\omega(1 - a \sin \omega t) + J_1(a) \cos \phi_0 + J_0(a) \cos \phi_0 \sin \omega t + J_0(a) \sin \phi_0 \cos \omega t + \dots \\
 & = \frac{I_1}{\cosh \gamma T} - 2F \sum_{n=1}^{\infty} (-1)^n e^{-2n\gamma T} \omega (1 - a \sin \omega(t - 2nT)).
 \end{aligned} \tag{24}$$

Collecting constant-in-time terms and terms proportional to $\sin \omega t$ and $\cos \omega t$ in Eq. (24), to the leading order, one finds

$$(2\beta + F \tanh \gamma T)\omega + J_1(a) \cos \phi_0 = \frac{I_1}{\cosh \gamma T}, \tag{25}$$

$$\omega \alpha_1(\omega) = \frac{J_0(a)}{a} \cos \phi_0, \tag{26}$$

$$\omega \alpha_2(\omega) = \frac{J_0(a)}{a} \sin \phi_0, \tag{27}$$

where

$$\alpha_1(\omega) \equiv 2\beta + \frac{F \sinh 2\gamma T}{\cosh 2\gamma T + \cos 2\omega T} \quad \text{and} \quad \alpha_2(\omega) \equiv \omega + \frac{F \sin 2\omega T}{\cosh 2\gamma T + \cos 2\omega T}.$$

One can recast Eqs. (25)–(27) in the form free from ϕ_0 :

$$(2\beta + F \tanh \gamma T)\omega + \omega \alpha_1(\omega) \frac{a J_1(a)}{J_0(a)} = \frac{I_1}{\cosh \gamma T}, \tag{28}$$

$$\frac{a}{J_0(a)} = \frac{1}{\omega \sqrt{\alpha_1^2(\omega) + \alpha_2^2(\omega)}}. \tag{29}$$

For given value of ω , Eq. (29) can be treated as a transcendental equation with respect to a . This equation possesses unique solution for a within the range from $a = 0$ to $2.4048\dots$, which is the first zero of the Bessel function $J_0(a)$. Since our derivations are valid for non-large a , we should restrict ourselves to the interior of the latter range. Thus, Eq. (29) dictates single-valued dependence of a on ω . With known $a(\omega)$, Eq. (28) yields the value of I_1 and Eq. (21) yields the value of V_1 . Summarising, the high-frequency solution is parameterised by frequency ω , which determines the amplitude a of phase oscillation via transcendental equation (29), and Eqs. (28) and (21) yield values of the corresponding input current I_1 and the time-average input voltage V_1 .

The case of low energy dissipation in resonator

Let us consider the case of $\gamma T \equiv \varepsilon \ll 1$ in detail. In this case, one can simplify:

$$\alpha_1 = 2\beta + \frac{F\varepsilon}{\varepsilon^2 + \cos^2 \omega T}, \quad \alpha_2 = \omega + \frac{F \tan \omega T}{1 + \varepsilon^2 \tan^2 \omega T},$$

The expression α_2 can turn to zero, which can result in resonantly high values of I_1 . Let us find frequencies ω , where α_2 attains zero value. Condition $\alpha_2 = 0$ yields

$$\omega + \varepsilon^2 \omega \tan^2 \omega T + F \tan \omega T = 0,$$

which can be viewed as a quadratic equation with respect to $\tan \omega T$. Hence, one can write

$$(\tan \omega T)_{1,2} = \frac{-F \pm \sqrt{F^2 - 4\omega^2 \varepsilon^2}}{2\varepsilon^2 \omega}.$$

For $\varepsilon \rightarrow 0$, these two branches of roots take the limiting forms:

$$\tan \omega_{1,n} T = -\frac{\omega_{1,n}}{F}, \quad (30)$$

$$\cot \omega_{2,n} T = -\frac{\varepsilon^2 \omega_{2,n}}{F}. \quad (31)$$

The roots of these equations are

$$\omega_{1,n} = \frac{\pi}{T} \left(n + \frac{1}{2} \right) + \frac{F}{\pi \left(n + \frac{1}{2} \right)} + \dots, \quad \omega_{2,n} = \frac{\pi}{T} \left(n + \frac{1}{2} \right) \left(1 + \frac{\varepsilon^2}{FT} + \dots \right).$$

For these roots, one finds

$$\alpha_1(\omega_{1,n}) \approx 2\beta + \frac{\varepsilon}{F}(F^2 + \omega_{1,n}^2), \quad \alpha_1(\omega_{2,n}) \approx 2\beta + \frac{F}{\varepsilon}.$$

At points where $\alpha_2 = 0$, Eq. (28) also simplifies to

$$I_1 = (2\beta + \varepsilon F)\omega + J_1(a). \quad (32)$$

One can see, that for the first group of roots, $\omega = \omega_{1,n}$, the value of α_1 is small and Eq. (29) yields non-small values of a . Hence, $J_1(a)$ makes a non-small correction to the trend $(2\beta + \varepsilon F)\omega$. Meanwhile, for the second group of roots, $\omega = \omega_{2,n}$, α_1 is large and, according to Eq. (29), a is small. Hence, $a(\omega_{2,n}) \approx (\omega\alpha_1)^{-1}$ and

$$I_1(\omega_{2,n}) \approx (2\beta + \varepsilon F)\omega_{2,n} + \frac{\varepsilon}{2\omega_{2,n}F}.$$

The increase of I_1 compared to the trend $(2\beta + \varepsilon F)\omega$ is small ($\propto \varepsilon$); there is no resonant peaks at $\omega_{2,n}$. Thus, there is a resonant increase of the input current I_1 at resonant frequencies $\omega = \omega_{1,n}$, this increase is especially strongly pronounced for small ohmic dissipation at the Josephson junction ($\beta \ll 1$).

The physical mechanism of the increase of the input current required to maintain oscillations with resonant frequencies is as follows. With no dissipation and at resonant frequency, one can excite in the resonator a standing wave with zeros at the boundaries. For small dissipation and frequency mismatch, there are hiers of the resonant standing wave, which are the oscillating patterns with nearly zero values of fields at the boundaries. When one maintains not small, but moderate values of the fields at the boundaries (which are, in our case, due to inherent dynamics of the Josephson junction and external input current), the patterns in resonator are proportionally increased and become large-amplitude. Hence, even for small values of dissipation coefficients, the dissipation at the resonator becomes non-small and one requires stronger energy supply to the system to maintain the regime with a resonant frequency. This energy is supplied to the system with external input current, which has to be consequently increased.

Comparison with numerical results and interpretation

In Figure 3, one can see the results of the analytical theory [Eqs. (21), (28), (29)] to match the results of numerical simulation well (the relative error of numerical simulations is below 10^{-12}). The analytical theory inaccurately estimates the height of one or two low-frequency resonant peaks (while their position with respect to V_1 and, therefore, frequency are predicted accurately) and misses the nonlinear resonances which are non-negligible in the same low-frequency domain of parameters. The nonlinear corrections to the analytical theory are derived in the next section and with these corrections the nonlinear resonances appear where they are observed with numerical simulations. However, in the low-frequency domain, the series with respect to powers of ω^{-1} does not converge at the centres of peaks and the weakly-nonlinear analytical theory does not describe the system behaviour; only the position of nonlinear resonances is predicted accurately.

It turns out that the analytical theory describes the resonant behaviour very well immediately above the low-frequency domain (see Figure 3).

The analytical solution provides steady states, which can be either stable or unstable. At the solution branching points the tangential bifurcation occurs meaning the one of solutions is stable while the other is unstable. Since in numerical simulations, one observes only stable solutions, we can surely conclude that for resonant peaks the lower branch is stable, while the upper one is unstable (see Figure 3). A small distance between stable and unstable branches on the current–voltage plane does not mean that the attraction basin of the stable state is small; the branches are close only in the projection to this plane, while in the full phase space they are well remote from each other. With arbitrary initial conditions, the system frequently arrives to the stable resonant states.

Nonlinear corrections of higher order

In this section we develop a perturbation analysis accounting for higher order terms. It will be convenient to read Eq. (18) in the form

$$\hat{L}\phi + \sin\phi = \frac{I_1}{\cosh\gamma T}, \quad (33)$$

where

$$\hat{L}\phi \equiv \phi_{tt}(t) + (2\beta + F)\phi_t(t) + 2F \sum_{n=1}^{\infty} (-e^{-2\gamma T})^n \phi_t(t - 2nT).$$

One can evaluate

$$\hat{L}\omega t = 2\beta\omega + F\omega \tanh\gamma T, \quad (34)$$

and

$$\begin{aligned} \hat{L}\phi_{\omega} = & \omega \cos\omega t \left[-\omega a_{\omega} + 2\beta b_{\omega} + \frac{F(-a_{\omega} \sin 2\omega T + b_{\omega} \sinh 2\gamma T)}{\cosh 2\gamma T + \cos 2\omega T} \right] \\ & + \omega \sin\omega t \left[-\omega b_{\omega} - 2\beta a_{\omega} + \frac{F(-b_{\omega} \sin 2\omega T - a_{\omega} \sinh 2\gamma T)}{\cosh 2\gamma T + \cos 2\omega T} \right]. \end{aligned} \quad (35)$$

where $\phi_{\omega} = a_{\omega} \cos\omega t + b_{\omega} \sin\omega t$.

After lengthy but straightforward calculations, one can find from Eq. (33), to the 3rd order,

$$I_1 = (2\beta \cosh\gamma T + F \sinh\gamma T)\omega + \cosh\gamma T \left(\frac{a_1^{(1)} + a_1^{(3)}}{2} + \frac{b_1^{(1)} a_2^{(2)} - b_2^{(2)} a_1^{(1)}}{4} - \frac{a_1^{(1)} [(a_1^{(1)})^2 + (b_1^{(1)})^2]}{16} \right) + \mathcal{O}(\omega^{-4}). \quad (36)$$

Where $a_n^{(k)}$ and $b_n^{(k)}$ are determined by the following linear equations:

$$\begin{pmatrix} \alpha_2(\omega) & -\alpha_1(\omega) \\ \alpha_1(\omega) & \alpha_2(\omega) \end{pmatrix} \begin{Bmatrix} a_1^{(1)} \\ b_1^{(1)} \end{Bmatrix} = \frac{1}{\omega} \begin{Bmatrix} 0 \\ 1 \end{Bmatrix}, \quad (37)$$

$$\begin{pmatrix} \alpha_2(2\omega) & -\alpha_1(2\omega) \\ \alpha_1(2\omega) & \alpha_2(2\omega) \end{pmatrix} \begin{Bmatrix} a_2^{(2)} \\ b_2^{(2)} \end{Bmatrix} = \frac{1}{4\omega} \begin{Bmatrix} a_1^{(1)} \\ b_1^{(1)} \end{Bmatrix}, \quad (38)$$

$$\begin{pmatrix} \alpha_2(\omega) & -\alpha_1(\omega) \\ \alpha_1(\omega) & \alpha_2(\omega) \end{pmatrix} \begin{Bmatrix} a_1^{(3)} \\ b_1^{(3)} \end{Bmatrix} = \frac{1}{\omega} \begin{Bmatrix} a_2^{(2)}/2 - a_1^{(1)}b_1^{(1)}/4 \\ b_2^{(2)}/2 - [(a_1^{(1)})^2 + 3(b_1^{(1)})^2]/8 \end{Bmatrix}. \quad (39)$$

The average value of the input voltage is determined by Eq. (21) exactly;

$$V_1 = I_1 \tanh 2\gamma T + \frac{F\omega}{\cosh \gamma T}.$$

Weakly-nonlinear solution (21), (36)–(39) provides corrections to the solution derived without accounting for 2ω - and higher harmonics. This solution is parameterised by frequency ω . The weakly nonlinear solution correctly pinpoints the position of nonlinear resonances which can be seen in Figure 3 (stripes without number n) for low frequencies which correspond to small average voltage V_1 . Unfortunately, the weakly nonlinear solution helps only with identification of the position of nonlinear resonant peaks and confirming their nature; it does not reproduce the shape of peaks well, because of the divergence of the expansion with respect to ω^{-1} at low frequency domain.

Conclusion

A high- Q circuit of a Josephson junction connected to resonator (a lengthy capacitor) has been found to exhibit multistability in regimes of operation and the current–voltage characteristic. The multistability is associated with tall peaks at the current–voltage characteristic emerging at generated oscillation frequencies which are resonant ones for a distributed parameter capacitor.

In resonant regimes, variation of the input current, which is a control parameter for this system in practice, makes a minor impact on the average input voltage and generation frequency. The resonant frequencies are given by Eq. (30), $\omega_{1,n} \approx (\pi/T)(n + 1/2)$, and the corresponding average voltage determined by Eq. (21) reads $V_{1,n} \approx (\pi F/T)(n + 1/2)$.

The detailed knowledge of features of the current–voltage characteristic we derived allows one to surely distinguish the resonant patterns we consider from the patterns reported for arrays of Josephson junctions reported by Barbara *et al.*⁹. Thus, the latter can be reliably recognized.

Considering Josephson junctions as natural voltage-to-frequency or current-to-frequency transducers, we would like to notice the possibility to strongly stabilize or efficiently control the generation frequency by means of a resonator. The stabilized generation frequencies are determined by generator properties; $\omega_{1,n} \approx (\pi/T)(n + 1/2)$, where T is the time of signal travel along the resonator.

References

1. B. D. Josephson, *Possible new effects in superconductive tunnelling*, Phys. Lett. **1**(7), 251–253 (1962).
2. G. F. Zharkov, Yu. K. Al'tudov, *Alternating-current Josephson effect*, Sov. Phys. JETP **47**(5), 901–906 (1978).
3. D. R. Tilley, *Superradiance in arrays of superconducting weak links*, Phys. Lett. **33A**(4), 205–206 (1970).
4. D. Rogovin, M. Scully, *Superconductivity and macroscopic quantum phenomena*, Phys. Rep. **25C**, 175–291 (1976).
5. J. Q. You, F. Nori, *Atomic physics and quantum optics using superconducting circuits*, Nature **474**(7353), 589–597 (2011).
6. A. K. Jain, K. K. Likharev, J. E. Lukens, J. E. Sauvageau, *Mutual phase-locking in Josephson junction arrays*, Phys. Rep. **109**, 309–426 (1984).
7. S. P. Benz, C. J. Burroughs, *Coherent emission from two-dimensional Josephson junction arrays*, Appl. Phys. Lett. **58**, 2162–2164 (1991).
8. K. Wiesenfeld, S. Benz, P. A. A. Booi, *Phase-locked oscillator optimization for arrays of Josephson junctions*, J. Appl. Phys. **76**, 3835–3846 (1994).
9. P. Barbara, A. B. Cawthorne, S. V. Shitov, C. J. Lobb, *Stimulated Emission and Amplification in Josephson Junction Arrays*, Phys. Rev. Lett. **82**(9), 1963–1966 (1999).
10. K. Edelman, O. V. Gendelman, *Dynamics of self-excited oscillators with neutral delay coupling*, Nonlinear Dyn. **72**, 683–694 (2013).
11. L. Ozyuzer, A. E. Koshelev, C. Kurter, N. Gopalsami, *et al.* *Emission of coherent THz radiation from superconductors*, Science **318**(5854), 1291–1293 (2007).
12. A. J. Berkley, H. Xu, R. C. Ramos, M. A. Gubrud, *et al.*, *Entangled macroscopic quantum States in two superconducting qubits*, Science **300**(5625), 1548–1550 (2003).

13. F. W. Strauch, Ph. R. Johnson, A. J. Dragt, C. J. Lobb, *et al.*, *Quantum logic gates for coupled superconducting phase qubits*, Phys. Rev. Lett. **91**(16), 167005 (2003).
14. J. Clarke, F. K. Wilhelm, *Superconducting quantum bits*, Nature **453**(7198), 1031–1042 (2008).
15. D. S. Goldobin, *Anharmonic resonances with recursive delay feedback*, Phys. Lett. A **375**, 3410–3414 (2011).

Acknowledgements

The idea of considering this problem was suggested by Prof. Arkady Pikovsky, to whom the authors are also grateful for seminal discussions of the work findings and useful comments on the manuscript. The authors acknowledge financial support by the Russian Science Foundation (Grant No. 14-21-00090).

Author contributions statement

All authors performed the analytical calculations and the theoretical analyses and participated in the writing of the manuscript. D.S.G performed the numerical simulation. All authors reviewed the final version of the manuscript.

Additional information

Competing financial interests The authors declare no competing financial interests.